
Proceedings Paper:
Markovic, U, Aristidou, P orcid.org/0000-0003-4429-0225 and Hug, G (2017) Virtual Induction Machine Strategy for Converters in Power Systems with Low Rotational Inertia. In: Proceedings of IREP'2017 Symposium. 10th Bulk Power Systems Dynamics and Control Symposium – IREP'2017, 27 Aug - 01 Sep 2017, Espinho, Portugal. IREP .

Virtual Induction Machine Strategy for Converters in Power Systems with Low Rotational Inertia

Uros Markovic*, Petros Aristidou§, Gabriela Hug*
* EEH - Power Systems Laboratory, ETH Zurich, Physikstrasse 3, 8092 Zurich, Switzerland
§ School of Electronic and Electrical Engineering, University of Leeds, Leeds LS2 9JT, UK
Emails: {markovic, hug}@eeh.ee.ethz.ch, p.aristidou@leeds.ac.uk

***Abstract*—This paper presents a novel comprehensive control strategy for grid-connected Voltage Source Converters (VSCs) in power systems with low rotational inertia. The proposed model is based on emulating the physical properties of an Induction Machine (IM) and taking advantage of its inherent grid-friendly properties, i.e. self-synchronization, virtual inertia, power and frequency oscillation damping. For that purpose, a detailed mathematical model of the IMs working principles is derived, which includes the possibility of obtaining the unknown grid frequency without a dedicated synchronization unit, but rather via processing the voltage and current magnitude measurements at the converter output. This eliminates the need for an inherently nonlinear phase-locked loop, characteristic for virtual synchronous machines, while simultaneously preserving the synchronization and damping properties of a conventional electrical machine. Several case studies are presented that validate the mathematical principles of the proposed model and conclusions on VSC performance are drawn.**

***Index Terms*—voltage source converter (VSC), induction machine, phase-locked loop (PLL), self-synchronization, virtual inertia emulation**

I. Introduction

Voltage Source Converters (VSCs) often represent the interface between the Distributed Generation (DG) and the grid. As a result, large-scale integration of Renewable Energy Sources (RES) has led to an increased share of Power Electronic (PE) devices in the power system. This can have a negative impact on the system stability margin due to the overall reduction of rotational inertia [1]–[3]. On the other hand, important questions regarding the operation and handling of converters in a power system with multiple traditional Electrical Machines (EM) have been raised over the previous years, in particular focusing on the unpredictable behavior of conventional PE control strategies in the presence of such machines [4]–[6]. One of the most common approaches to resolving the associated faster frequency dynamics and larger deviations in the system is through alternative converter control concepts that would reproduce the stabilizing behavior of the decreasing rotational inertia. Assuming that in the future the grid would consist of both machine- and PE-based units, the idea of deriving a unified control configuration for both unit types so that the grid experiences them in a similar fashion prevails as the most investigated approach in the literature [7]–[13]. These studies present somewhat similar variations of the common emulated Synchronous Machine (SM), defined as: synchronous VSC [7], virtual synchronous generator [8], [10], virtual SM [9], synchronous converter [11], [13] and VISMA [12]. Alternatively, the approach in [14] aims at replicating the characteristics of a VSC in a synchronous generator. However, all of the aforementioned methodologies result in the same undesirable effects due to the properties of SM, such as a need for a synchronization unit, potential of frequency hunting and insufficient saturation of fault currents [15].

In order to regulate a grid-connected inverter as a voltage source, a control sequence consisting of a synchronization unit, an outer power loop and a cascade of inner voltage and current control loops has become an industry standard for providing adequate voltage, active and reactive power outputs [16]. Furthermore, the norm of having a Phase-Locked Loop (PLL) as a synchronization unit has been established [17], together with its numerous variants [18], [19]. However, despite being widely used, this additional, inherently nonlinear, outer loop introduces complexity and time delay into the original control system and may be extremely difficult to tune [20], [21]. Recent studies have addressed this issue and concepts of PLL-less converter regulation in the form of power-synchronization [22] and self-synchronizing synchronverters [21] have emerged. While seemingly providing synchronization properties, the proposed methods also have some downsides. The power-synchronization is mostly oriented towards VSC-HVDC applications and faces challenges with weak AC system connections, whereas the synchroverter concept still requires a back-up PLL and improvements in operation under unbalanced and distorted grid voltages.

A recently proposed VSC control method under the name of *inducverter* introduces the idea of a grid-connected converter operating under Induction Machine (IM) working principles and no dedicated PLL unit [23]. Although the concept is still at its early stages, it can potentially resolve the issues associated with the conventional outer synchronization loop, while still preserving the damping and synchronization properties of a virtual inertia. This work reformulates the mathematical principles of a virtual machine from [23] and

This project has received funding from the *European Union's Horizon 2020 research and innovation programme* under grant agreement No 691800. This paper reflects only the authors' views and the European Commission is not responsible for any use that may be made of the information it contains.

extends on it in several directions by: (i) integrating it on top of the fully developed VSC droop control (ii) implementing a complete inner control sequence instead of an adaptive lead/lag compensator; and (iii) re-orienting the frame control from a hybrid (abc/dq) to a synchronously rotating (dq)-frame. First, we propose a detailed control configuration of a voltage source-operated converter regulated as an IM, based on its electromechanical principles, and adjusted for the potential VSC modes of operation. Second, a detailed converter control model is incorporated and tested in a simulation environment, which enables us to draw adequate conclusions regarding the overall emulation properties and the system response.

The remainder of the paper is structured as follows. In Section II, a detailed mathematical model of a VIM is presented. Section III describes the properties of a VSC emulated as an IM and proposes a comprehensive control scheme. Section IV showcases the preliminary results of transient simulations, whereas Section V discusses the outlook of the study and concludes the paper.

II. Virtual Induction Machine Model

A. Induction vs Synchronous Machine: Working Principles

One of the main differences between the synchronous and induction machine is the physical concept behind the rotor movement and the subsequent synchronization to the grid. While the SM always operates at synchronous speed, the IM requires a mismatch between the synchronous and the machine speed to operate, a so-called slip (ν):

$$\nu = \frac{\omega_s - \omega_r}{\omega_s} = \frac{\omega_\nu}{\omega_s} \tag{1}$$

Furthermore, unlike synchronous generators, induction machines do not have an excitation system in the rotor. This means that the ElectroMagnetic Field (EMF) induced in the rotor of an IM is a consequence of its rotation and the subsequent change of the magnetic flux linkage through the circuit. Since the rotor is closed through either an external resistance or a short-circuit ring, the induced EMF generates a current flow in the rotor conductor. Therefore, the machine can never be operating at the synchronous speed, since there would be no EMF in the rotor frame to initiate its movement.

Based on the previously described properties, one can observe that the IM with an arbitrary initial rotor speed somewhat close to the synchronous speed has self-start capability, i.e. has the potential to synchronize with a grid of an unknown frequency and voltage magnitude. This implies that the PLL units, together with their inherent downsides in the form of time delay and stability margins, could be avoided from the converter model. Nonetheless, all of the advantageous inertia properties, such as power and frequency oscillation damping, can be appropriately reproduced via a closed-loop converter control.

B. Induction Machine Emulation Concept

For the purpose of emulating the operating principles of an IM through VSC control, let us observe the model of an IM in a synchronous (dq)-frame [24]:

$$v_s^d = R_s i_s^d + \dot{\psi}_s^d - \omega_s \psi_s^q \tag{2}$$

$$v_s^q = R_s i_s^q + \dot{\psi}_s^q + \omega_s \psi_s^d \tag{3}$$

$$v_r^d = 0 = R_r i_r^d + \dot{\psi}_r^d - \omega_\nu \psi_r^q \tag{4}$$

$$v_r^q = 0 = R_r i_r^q + \dot{\psi}_r^q + \omega_\nu \psi_r^d \tag{5}$$

where v_s, v_r, ψ_s, ψ_r are respectively the stator and rotor voltages and flux linkages. The superscripts d and q refer to the corresponding axis of the (dq)-reference frame, rotating at the time-variant synchronous speed ω_s. Based on the aforementioned equivalent circuit model, the set of equations for the stator and rotor flux linkages can be defined as:

$$\boldsymbol{\psi}_s = L_s \boldsymbol{i}_s + L_m \boldsymbol{i}_r \tag{6}$$

$$\boldsymbol{\psi}_r = L_r \boldsymbol{i}_r + L_m \boldsymbol{i}_s \tag{7}$$

with vectors $\boldsymbol{\psi}_s^T = \left[\psi_s^d,\, \psi_s^q\right]$, $\boldsymbol{\psi}_r^T = \left[\psi_r^d,\, \psi_r^q\right]$, $\boldsymbol{i}_s^T = \left[i_s^d,\, i_s^q\right]$ and $\boldsymbol{i}_r^T = \left[i_r^d,\, i_r^q\right]$ denoting the flux linkage and current components in different axes. Finally, the electric power passing between stator and rotor can be expressed in the following form:

$$p_e = \omega_s \frac{3}{2}\left(\psi_s^d i_s^q - \psi_s^q i_s^d\right) = \omega_s \frac{3}{2}\left(\psi_r^q i_r^d - \psi_r^d i_r^q\right) \tag{8}$$

which yields the virtual electrical torque

$$\tau_e = \frac{p_e}{\omega_s} = \frac{3}{2}\left(\psi_s^d i_s^q - \psi_s^q i_s^d\right) = \frac{3}{2} L_m \left(i_r^d i_s^q - i_r^q i_s^d\right) \tag{9}$$

It can be observed that the expression of τ_e in (9) is the same as a synchronous machine [24].

While the synchronous speed (ω_s) appears in (2)-(5), the control concept proposed in [23] does not include a PLL device. Therefore, ω_s is an unknown variable that needs to be computed. For that purpose, a field-oriented IM control, first presented in [25], is employed expressing ω_s as a function of other system parameters. Since the direction of the (dq)-frame is arbitrary, it is assumed that in steady state the virtual rotor flux is aligned with the d-axis, resulting in a simplified model with $\psi_r^q = 0$. The described procedure is similar to ones used in conventional PLLs, where the calculation of the voltage angle is based on aligning the voltage vector with the d-axis of the synchronous reference-frame [26]. Having in mind the suggested approximation, (7) is reformulated as:

$$i_r^d = \frac{\psi_r^d - L_m i_s^d}{L_r} \tag{10}$$

$$i_r^q = -\frac{L_m}{L_r} i_s^q \tag{11}$$

Furthermore, the expressions for rotor voltage components in (4) and (5) can now be rewritten as:

$$0 = R_r i_r^d + \dot{\psi}_r^d \tag{12}$$

$$0 = R_r i_r^q + \omega_\nu \psi_r^d \tag{13}$$

Substituting (10) into (12) and applying the Laplace transform yields:

$$\dot{\psi}_r^d = -R_r i_r^d = -\frac{R_r}{L_r}\left(\psi_r^d - L_m i_s^d\right) \overset{\mathcal{L}}{\longmapsto}$$
$$\psi_r^d = \frac{R_r L_m}{R_r + sL_r} i_s^d = K_\psi i_s^d \tag{14}$$

In a similar fashion, the virtual slip of the IM is computed by combining equations (11), (13) and (14):

$$\begin{aligned} \omega_\nu &= -\frac{R_r}{\psi_r^d} i_r^q = -\frac{R_r L_m}{L_r}\frac{i_s^q}{\psi_r^d} \overset{\mathcal{L}}{\longmapsto} \\ \omega_\nu &= \left(\frac{R_r}{L_r} + s\right)\frac{i_s^q}{i_s^d} = K_\nu \frac{i_s^q}{i_s^d} \end{aligned} \tag{15}$$

The final term[1] in (15) describes the dynamics of the frequency slip, which is adaptable to the variations in grid frequency and machine power output. However, an exact estimation of the rotor angle and frequency is necessary to remove the PLL and completely replace its functions. This can be achieved by observing the swing equation of a VIM and obtaining the mechanical dynamics of the rotor:

$$J\dot{\omega}_r = \tau_m - \tau_e - \tau_d \tag{16}$$

where J is the virtual rotor's momentum of inertia, and τ_m, τ_e and τ_d correspond to the mechanical, electrical and damping torque. If we set $\Delta\omega_r$ as deviation of ω_r from an initial value ω_0, the expression (16) becomes:

$$\Delta\dot{\omega}_r = \frac{1}{J}\left(\tau_m - \tau_e - \tau_d\right) \tag{17}$$

The electrical torque component is defined in (9), but can be further simplified by substituting the expressions of stator flux linkage components:

$$\psi_s^d = \left(L_s - \frac{L_m^2}{L_r}\right) i_s^d + \frac{L_m}{L_r}\psi_r^d \tag{18}$$

$$\psi_s^q = \left(L_s - \frac{L_m^2}{L_r}\right) i_s^q \tag{19}$$

Equations (18) and (19) are obtained from (6) and (7). The electrical torque is now reformulated as follows:

$$\tau_e = \frac{3}{2}\frac{L_m}{L_r}\psi_r^d i_s^q \overset{\mathcal{L}}{\longmapsto} \tau_e = K_e i_s^d i_s^q \tag{20}$$

where

$$K_e = \frac{3}{2}\frac{L_m}{L_r}K_\psi = \frac{3}{2}\frac{R_r L_m^2}{R_r L_r + sL_r^2} \tag{21}$$

The mechanical torque is determined by the inverter mechanical power input and the angular speed of the rotor. Assuming a lossless converter, the input power can be approximated by the output power measured at the converter terminal (p), as given by:

$$\tau_m = \frac{p_m}{\omega_r} \approx \frac{p}{\omega_r} \tag{22}$$

[1]The notation (s) of complex variable terms in frequency domain is omitted from equations for simplicity.

Finally, the damping torque is proportional to the rotor frequency deviation:

$$\tau_d = K_d \Delta\omega_r \tag{23}$$

which yields the following low-pass filter characteristic of the VIM in the frequency domain:

$$\Delta\omega_r = \frac{1}{Js + K_d}\left(\tau_m - \tau_e\right) \tag{24}$$

Similar to the synchronous machine model, the damping factor K_d represents an equivalent of the VM to the active power droop. The synchronous speed and angle reference can be obtained from ω_0, ω_ν, and $\Delta\omega_r$, as follows:

$$\omega_r = \omega_0 + \Delta\omega_r \tag{25}$$

$$\omega_s = \omega_r + \omega_\nu \tag{26}$$

$$\dot{\theta} = \omega_s \overset{\mathcal{L}}{\longmapsto} \theta = \frac{1}{s}\left(\omega_0 + \Delta\omega_r + \omega_\nu\right) \tag{27}$$

Based on the model described by (21)-(27), it is shown that the closed-loop controller adequately emulates the inertia and damping of an IM, based only on the voltage ($\boldsymbol{v}_c$) and current ($\boldsymbol{i}_c$) measurements at the converter terminal. Furthermore, it provides synchronization properties through computing the voltage angle and frequency reference necessary for the Park transformation, thus fully replacing the conventional PLL.

Equations (25)-(27) reflect the working principles of an IM and show that the difference between the synchronous and initial rotor frequency can have a significant impact on the frequency deviation. The proper selection of ω_0 prior to the grid connection of the VSC reduces $\Delta\omega_r$ and the subsequent transients. This concept resembles the behavior of an induction generator in a similar operation mode [23]. It can be reasonably assumed that the VSC is connected to the grid during steady-state operation. Thus, a very basic PLL can be used only to estimate ω_0. However, even if this functionality is not available, any reasonable ω_0 will still allow the VIM to synchronise, while introducing some transients (as shown in Section IV-B).

III. VSC Control Scheme

An overview of the VIM model is shown in Fig. 1, where the VSC is connected to the grid through an RLC filter and a phase reactor. The output voltage angle and magnitude references are generated by an outer active and reactive power controller, respectively. The reference voltage vector signal is sent to the inner control loop consisting of cascaded voltage and current controllers operating in a Synchronously-rotating Reference Frame (SRF).

The distinction from a virtual SM model lies in the Virtual Machine Emulator (VME). The standard SM emulation techniques control the active power output of the converter in such a way that it replicates the reduced mathematical model of a synchronous machine, i.e. emulating the inertial characteristic and damping. These terms are incorporated into the swing equation together with the actual grid frequency measured with a PLL. On the contrary, the proposed VIM approach

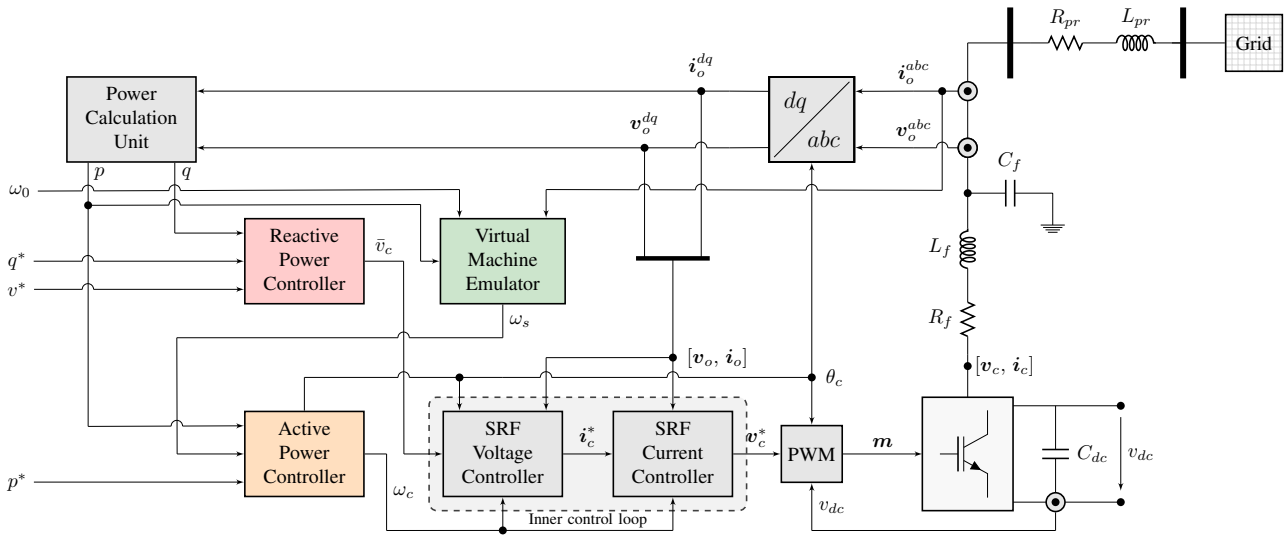

Fig. 1: VSC control scheme for an emulated induction machine.

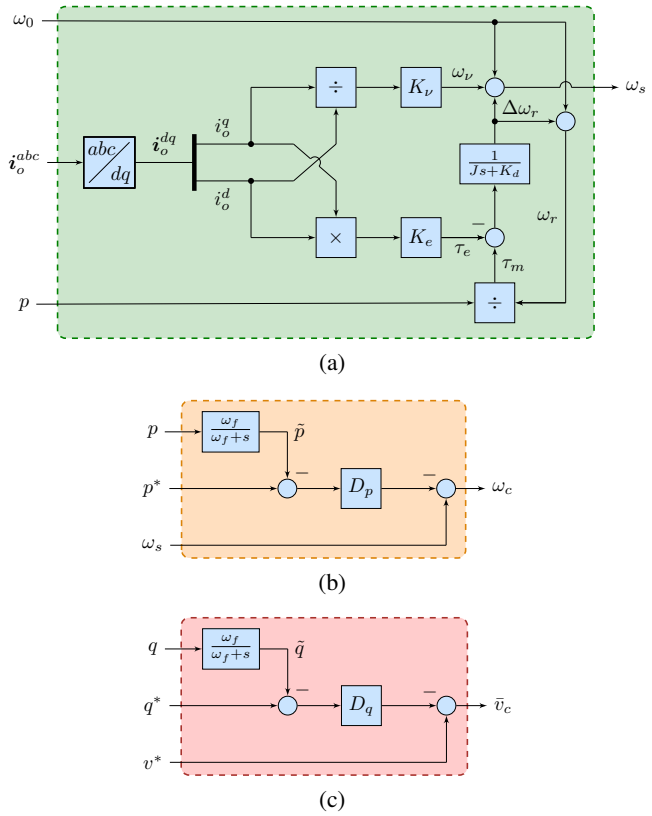

Fig. 2: Main control blocks of an induction machine emulator: (a) Virtual machine emulator. (b) Active power controller. (c) Reactive power controller.

incorporates a more stable VME loop and decouples it from the actual power controllers, as described in Section III-A.

Furthermore, it can be observed in Fig. 1 that the SRF orientation of the inner control loop is independent of any synchronization device as it is determined by the balancing mechanism of the inertial response [27]. The configuration of the aforementioned main control blocks is depicted in Fig. 2 and the mathematical reasoning behind it is elaborated in more detail below [9], [23], [28].

A. Virtual Machine Emulator

This block represents the central emulation unit of a VIM. It generates the internal frequency reference used as an input for the Active Power Controller (APC), thus eliminating the need for a PLL. The control design is based on eqs. (15), (20)-(24) and presented in Fig. 2a. One of the main advantages of this approach is that the unknown grid frequency can be obtained by simply measuring the current ($\boldsymbol{i}_o^{abc}$) and active power (p) magnitudes, i.e. current and voltage at the filter output terminal ($\boldsymbol{i}_o^{abc}$, $\boldsymbol{v}_o^{abc}$). Thus, the drawbacks of using a PLL unit for frequency estimation are resolved. Another necessary input for the VME is the initial rotor frequency (ω_0), which determines the IM oscillation level at start-up. However, the requirements for the value of ω_0 are not very strict, as it should only be "close enough" to the synchronous speed and subsequently let the emulated physical machine properties bring the VSC to synchronism. Besides replicating the synchronization capabilities, VME also provides current and power damping properties, all unified within a single control block. Unlike the most virtual SM models, this configuration fully decouples active power and inertia/damping emulation controls.

B. Active Power Controller

Droop control closely represents the relationship between the frequency and active power, and is therefore traditionally used as a method of controlling the converter's active power output in order to slow down and stabilize frequency deviation in case of a disturbance. Alternatively, various control methods derived from the swing equation and the corresponding power-balancing and oscillation-damping properties could be

employed [28]–[30]. However, it has been proven that a low-pass-filtered droop regulator with a constant angular frequency and active power setpoint is equivalent to the VSM model based on swing equation, with no filtering corresponding to a machine of zero inertia [9]. Due to the presence of an explicit synchronization loop, and in contrast to the work in [28], the proposed concept is implemented only through a power-frequency droop. Hence, the APC depicted in Fig. 2b is designed as a droop gain (D_p) imposed onto the difference between the setpoint (p^*) and the filtered power measurement ($\tilde{p}$):

$$\omega_c = \omega_s - D_p \cdot (p^* - \tilde{p}) \tag{28}$$

The controller's output (ω_c, θ_c) is then further used as an indicator of the SRF orientation in both inner and outer control loops.

C. Reactive Power Controller

The reactive power regulation consists of a simple droop controller described by (29)

$$\bar{v}_c = v^* - D_q \cdot (q^* - \tilde{q}) \tag{29}$$

and shown in Fig. 2c. The Reactive Power Controller (RPC) determines the initial voltage magnitude reference of a VSC terminal ($\bar{v}_c$) using a droop gain (D_q) and a deviation between the filtered reactive power measurement ($\tilde{q}$) and the external reactive power reference (q^*) signal.

D. Inner Control Loop and Modulation

The configuration of a VIM control scheme based on providing a voltage reference output is advantageous due to its explicit and decoupled active and reactive power controllers. However, a direct use of such signal for Pulse-Width Modulation (PWM) raises problems regarding the limitations and controlled saturation of the converter's currents and voltages [9]. These issues are conveniently resolved with a cascaded inner control scheme where the initial reference ($\bar{\boldsymbol{v}}_c$) is processed through a sequence of voltage and current loops, yielding a more robust converter setpoint ($\boldsymbol{v}_c^*$). This approach increases the flexibility of protection strategies and is commonly used in droop-controlled microgrids [31], [32].

Assuming an RLC-type filter connecting the converter and the phase reactor, the state-space equations of the converter's terminal voltage and current components are derived in the (dq)-frame:

$$\boldsymbol{v}_c = \boldsymbol{v}_o + L_f \dot{\boldsymbol{i}}_c + R_f \boldsymbol{i}_c \tag{30}$$

$$\boldsymbol{i}_c = \boldsymbol{i}_o + C_f \dot{\boldsymbol{v}}_o \tag{31}$$

where L_f, R_f, and C_f are the static filter parameter. The configuration of the inner cascade loops and the modulation block is derived from (30)-(31) and detailed below.

1) SRF Voltage Controller: The structure of the SRF voltage controller follows the same principles as the controllers in [9], [28]:

$$\boldsymbol{i}_c^* = K_f^i \boldsymbol{i}_o + (\bar{\boldsymbol{v}}_c - \boldsymbol{v}_o)\left(K_p^v + \frac{K_i^v}{s}\right) + \omega_c C_f \hat{\boldsymbol{v}}_o \tag{32}$$

where $\hat{\boldsymbol{v}}_o^T = \left[-v_o^q,\, v_o^d\right]$. We use a standard PI controller, with K_p^v and K_i^v being respectively the proportional and integral gains, to minimize the error between the setpoint ($\bar{\boldsymbol{v}}_c$) and the output voltage ($\bar{\boldsymbol{v}}_o$). Furthermore, a feed-forward signal of the measured currents can be enabled or disabled by changing the gain $K_f^i \in [0,\, 1]$. The output current reference ($\boldsymbol{i}_c^*$) is then used as an input setpoint to the current controller.

2) SRF Current Controller: Similar to its voltage counterpart, the configuration of the SRF current controller is based on a PI control with decoupling terms:

$$\boldsymbol{v}_c^* = K_f^v \boldsymbol{v}_o + (\boldsymbol{i}_c^* - \boldsymbol{i}_o)\left(K_p^i + \frac{K_i^i}{s}\right) + \omega_c L_f \hat{\boldsymbol{i}}_o \tag{33}$$

where K_p^v, K_i^v and K_f^v are the controller gains, and $\hat{\boldsymbol{i}}_o^T = \left[-i_o^q,\, i_o^d\right]$. The generated output voltage reference ($\boldsymbol{v}_c^*$) is used to determine the final modulation signal as explained in the next subsection.

3) Pulse-Width Modulation: For the purpose of an actual implementation of the VSC switching sequence, the voltage reference signal ($\boldsymbol{v}_c^*$) from the current controller must be processed and converted into the modulation index ($\boldsymbol{m}$). This can be achieved through means of instantaneous averaging applied to the output voltage of the converter. Furthermore, the time delay effect of PWM is neglected, which yields the following expression:

$$\boldsymbol{m}^{abc} = (\boldsymbol{T}_p \boldsymbol{T}_c)^{-1} \boldsymbol{m}^{dq} = (\boldsymbol{T}_p \boldsymbol{T}_c)^{-1} \frac{\boldsymbol{v}_c^*}{v_{dc}} \tag{34}$$

$$\boldsymbol{T}_c = \sqrt{\frac{2}{3}} \begin{bmatrix} 1 & -\frac{1}{2} & -\frac{1}{2} \\ 0 & \frac{\sqrt{3}}{2} & -\frac{\sqrt{3}}{2} \end{bmatrix} \tag{35}$$

$$\boldsymbol{T}_p = \begin{bmatrix} \cos\theta^{\alpha\beta} & \sin\theta^{\alpha\beta} \\ -\sin\theta^{\alpha\beta} & \cos\theta^{\alpha\beta} \end{bmatrix} \tag{36}$$

where $\boldsymbol{T}_c$ and $\boldsymbol{T}_p$ denote the Clarke and Park transformation matrices used for converting the voltage measurements into the (dq)-frame. The inclusion of the DC voltage (v_{dc}) enables the averaging and ensures that the actual VSC output is close to the initial reference. Additionally, it reduces the AC side sensitivity to the oscillations of the DC voltage [28].

IV. Results

In this section, the performance of the proposed control scheme is studied for various modes of operation. For this purpose, an averaged converter model was implemented in MATLAB Simulink with the use of SimPowerSystems toolbox for modeling the external components (network lines, loads, etc.). The full parameters of the converter used are given in Table I.

TABLE I: VIM Simulation Parameters

Parameter	Symbol	Value
Nominal active power	P_n	1 GW
Nominal ph-ph voltage	V_n	320 kV
DC link voltage	V_{dc}	640 kV
Nominal frequency	f_n	50 Hz
Inertia constant	H	5 s
Damping constant	K_d	10 $\frac{\text{Nm}}{\text{rad/s}}$
Rotor resistance	R_r	0.0005 p.u.
Rotor inductance	L_r	0.05 p.u.
Mutual inductance	L_m	0.6 p.u.
Active droop gain	D_p	0.02 p.u.
Reactive droop gain	D_q	0.001 p.u.

The response of the VM is highly dependent on the selection of the equivalent physical machine parameters. This mainly refers to the rotor resistance and inductance, as well as the mutual inductance included in the controller transfer function K_e. Additionally, proper inertia and damping constants are crucial to correctly calculate the rotor frequency. In turn, this affects the sinusoidal nature of the voltage and current at the converter output terminal. To select the parameters of the VIM, we have used the properties of a 1.5 MW wind turbine induction generator (type-1 wind turbine) and scaled-up its per unit parameters accordingly.

The dynamics of the frequency slip are described via K_ν in (15) and modelled with PD block. The proportional and derivative gains are $K_\nu^p = R_r/L_r$ and $K_\nu^d = 1$, respectively. During the transient response of the converter, the current derivative gain can be extremely high and destabilize the model. This problem is overcome by employing the Ziegler-Nichols method [33] for tuning of a PD controller, i.e. determining the optimal K_ν^d component, while assuming the same proportional gain K_ν^p. As a result, an optimal gain of $K_\nu^d = 0.01$ has been computed and used throughout this study. The parameters of the PI controllers in the inner voltage and current control loops have been kept the same as for the standard VSC operating mode, since their time constants drastically differ from the ones in the outer controllers and eliminate any potentially disruptive interactions. Furthermore, it enables us to test the plug-n-play properties of the virtual emulator.

The remainder of this section focuses on analyzing the transient behavior of the proposed VIM during various operations, such as start-up and synchronization, response to setpoint variation and voltage and power reference tracking. Finally, the impact of the initial rotor speed estimate (ω_0) on the converter synchronization process with the grid is studied.

A. Start-up and Synchronization

In this subsection, the connection of a VSC to the grid is studied. The converter is connected to the grid at $t = 0$ s, while the initial rotor frequency is assumed to be $f_0 = 50$ Hz, same as the grid frequency. The voltage reference is initialized at $v^* = 1$ p.u., whereas the active and reactive power setpoints are $p^* = 0.5$ p.u. and $q^* = 0$ p.u., respectively.

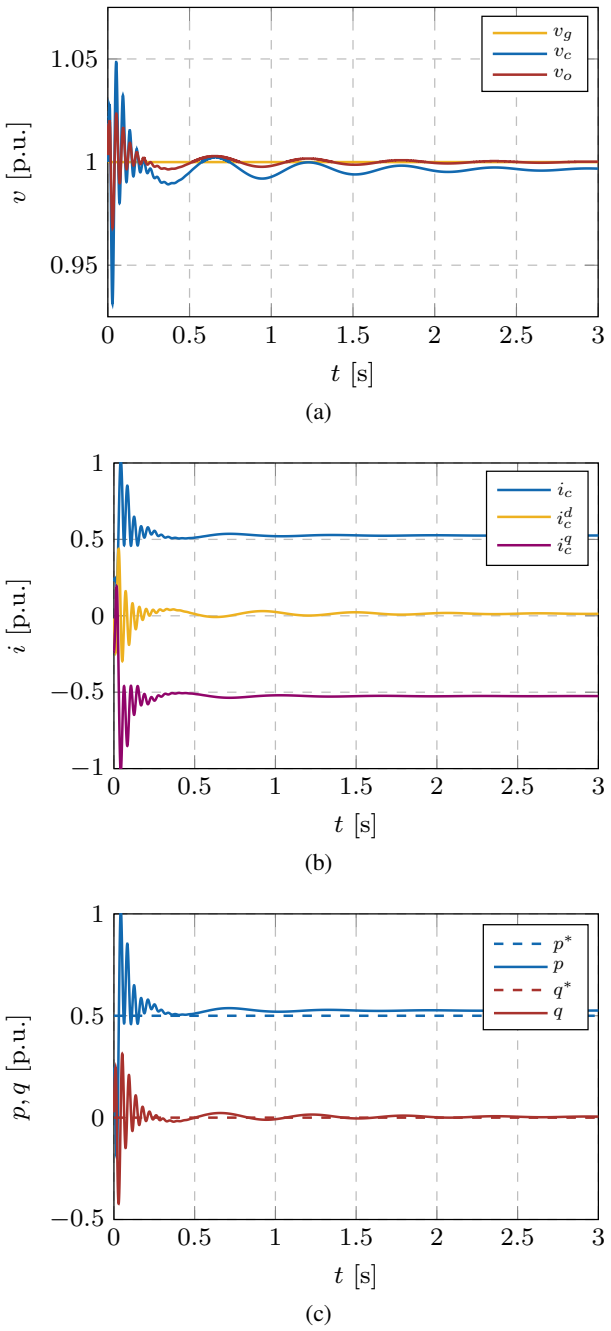

Fig. 3: Behavior of the converter emulated as a virtual induction machine during start-up: (a) RMS output voltages (before and after the filter). (b) RMS output current with dq-components. (c) Active and reactive power output and reference tracking.

Figure 3 confirms the soft-start and self-synchronization capabilities of the VIM, as well as an adequate damping characteristic. The setpoints are correctly followed and the voltage and current overshoots during start-up are acceptable. Furthermore, the initial transient response can be explained by observing the estimated synchronous frequency and its components in Fig. 4. As shown in Fig. 4b, the frequency slip term (f_ν) is very volatile during the first 100 ms, unlike

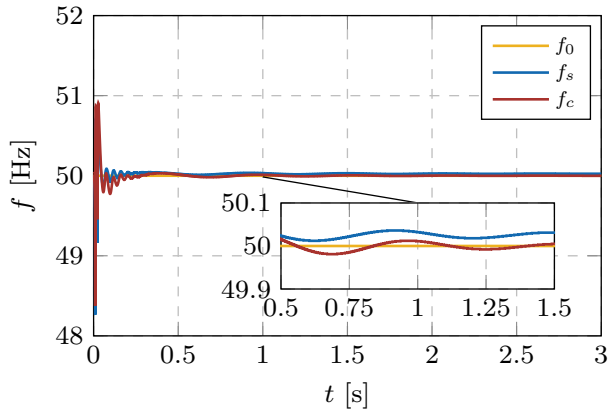

(a)

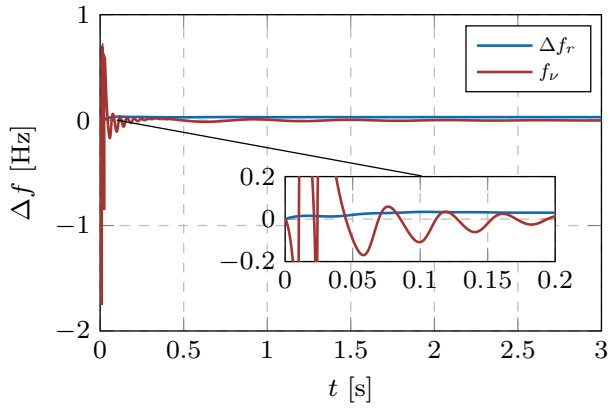

(b)

Fig. 4: Frequency response of the virtual machine emulator during start-up: (a) Initial and computed frequency terms. (b) Contribution of different frequency components.

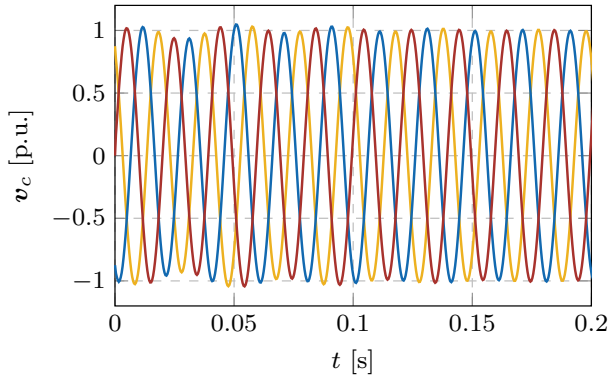

(a)

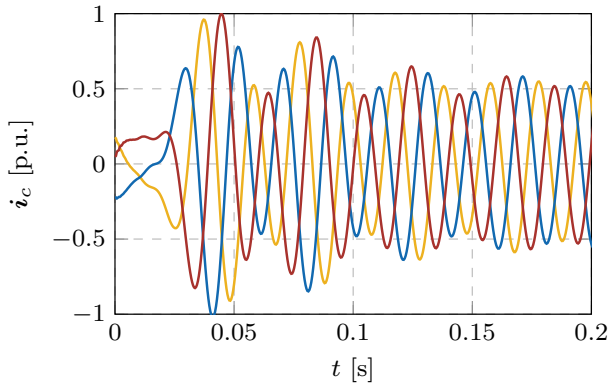

(b)

Fig. 5: Three-phase components at the converter output during start-up: (a) Instantaneous output voltages. (b) Instantaneous output currents.

the rotor frequency dynamics term (Δf_r). This is due to two reasons: (i) frequency slip is proportional to the quotient i_s^q/i_s^d, which can reach very high values when $i_c^d \approx 0$; (ii) K_ν behaves as a PD controller, with its derivative actions (K_ν^d) being mostly used throughout the first 100 ms of the start-up. After 400 ms both frequency components stabilize and the synchronous frequency reaches a steady state value of $f_s \approx 50.03$ Hz, whereas the active power droop controller brings it back to the nominal value (f_c).

The initial VSC overcurrent response shown in Fig. 5b follows the characteristic response of an IM and the synchronization of all three phases is achieved within ten cycles. Additionally, the lack of a PLL unit simplifies the model and eliminates potential instabilities caused by the synchronization loop. It can be concluded that, unlike the conventional synchronization approaches, this strategy enables the controller to easily track the predefined setpoints immediately after the start-up process. Nonetheless, it should also be pointed out that, despite following the reference, the active power output of the converter will never be exactly the same as the setpoint p^*, but rather have a small steady-state mismatch. The reason for this can be explained by observing (28) and Fig. 4, which indicates that the frequencies ω_s and ω_c are not identical and, therefore, lead to a small difference between the active power measurement and the respective setpoint.

B. Sensitivity to estimated initial frequency

One of the requirements of the proposed VME block is the estimation of the initial rotor frequency, denoted as f_0. In the previous example, it was shown that assuming $f_0 = f_n$ leads to a very responsive system with good synchronization and damping properties. However, having knowledge of the exact grid frequency prior to the connection of the VSC might not be feasible. Thus, the impact of selecting f_0 different from the real grid frequency is studied in this subsection.

The f_0 values of 50 Hz, 49.9 Hz and 50.1 Hz have been used and the corresponding behavior of the VIM is depicted in Fig. 6. While the synchronous speed computed through the VME unit tends to stay closer to f_0, the final frequency term resulting from an active power droop control eventually synchronizes with the grid. This confirms that for f_0 inputs that are both reasonably higher and lower that the actual grid frequency, the synchronization properties of VIM remain stable during start-up.

C. Setpoint Variation and Reference Tracking

Another important aspect of the controller performance is the reference tracking capability, such as a voltage reference

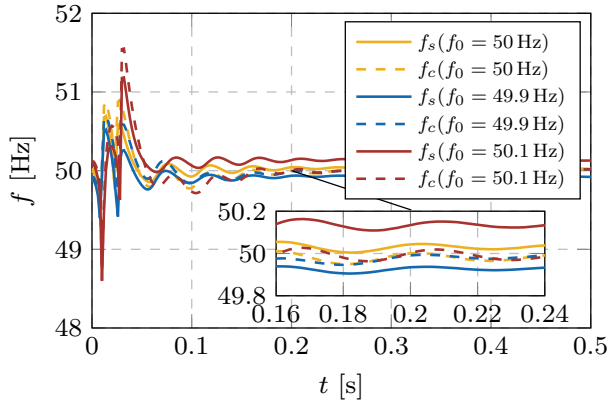

(a)

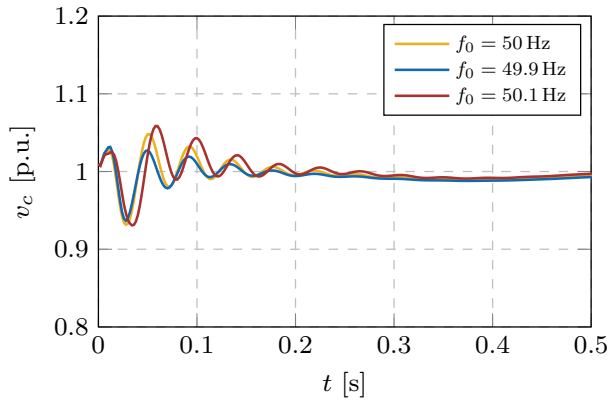

(b)

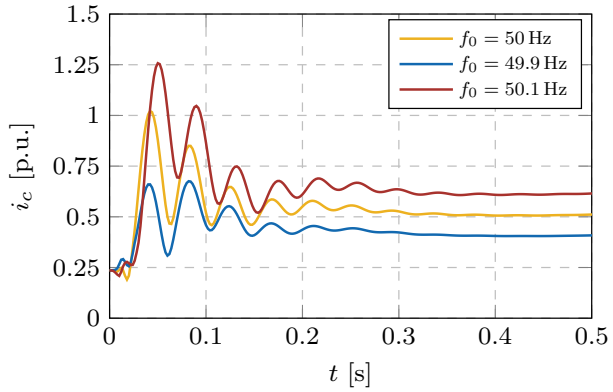

(c)

Fig. 6: Impact of initial rotor frequency term on the synchronization process of a VIM during start-up: (a) Frequency. (b) Output voltage. (c) Output current.

variation or a step change in the active power setpoint. Both scenarios are presented in Fig. 7, with setpoint changes occurring at $t = 0.25\,\text{s}$ in each case. The voltage reference is suddenly increased by $5\,\%$, whereas the active power reference spikes from $p^* = 0.5\,\text{p.u.}$ to $p^* = 0.6\,\text{p.u.}$, i.e. $20\,\%$. Both steps last for $1.25\,\text{s}$, before returning to the initial values.

The voltage response in Fig. 7a shows that the output voltage (v_o) follows the reference change. Some transient behaviour is observed for a short period of time ($\approx 200\,\text{ms}$)

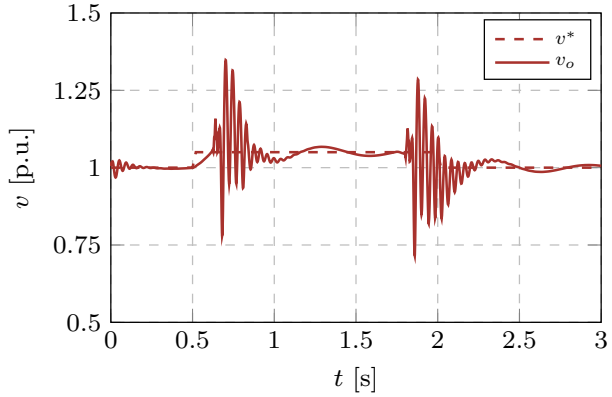

(a)

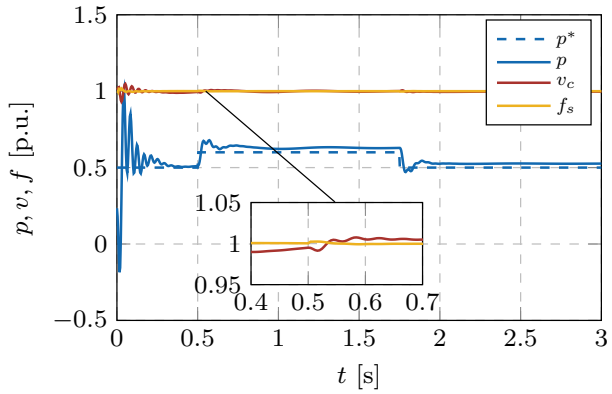

(b)

Fig. 7: VIM response to the variation of controller setpoints: (a) Variation of the voltage setpoint. (b) Variation of the active power setpoint.

but the voltage stabilizes around the predefined setpoint value. At the same time, the voltage and frequency spikes during the step change of active power setpoints are almost negligible. Similar to the previous case study, the power output follows the reference with a small steady state error.

V. Conclusion

In this paper, a novel control strategy for grid-connected VSCs with the use of induction generator emulation has been proposed. In particular, a detailed IM mathematical model was derived, together with a corresponding converter control scheme. The proposed approach eliminates the need for a dedicated PLL unit, while simultaneously preserving the synchronization and damping properties of a virtual induction machine. It can easily be integrated with the existing inner and outer converter control loops, without any negative interactions, due to its universal design and plug-n-play characteristics.

Several test cases have been conducted and the following promising conclusions can be drawn: The start-up of the VIM and the synchronization with the grid are smooth, with reasonably small current overshoots. The computation of all frequency components is accurate, even when the initial rotor speed is not equal to the grid frequency, whereas the predefined

voltage and power setpoints are met in the steady state. This reference tracking property is fulfilled even during sudden step changes in the setpoint input.

Further work on this topic will extend the analysis on VSC's control response and investigate it in a wider range of operating conditions, including disturbances on a DC side and grid synchronization under unbalanced conditions. Furthermore, the interactions between the VIM and the conventional electrical machines in the system should to be studied in more detail, with a special focus on the grid-following properties of the proposed converter.

REFERENCES

[1] A. Ulbig, T. S. Borsche, and G. Andersson, "Impact of Low Rotational Inertia on Power System Stability and Operation," *ArXiv e-prints*, Dec. 2013.

[2] J. G. Slootweg and W. L. Kling, "Impacts of distributed generation on power system transient stability," in *IEEE Power Engineering Society Summer Meeting,*, vol. 2, July 2002, pp. 862–867 vol.2.

[3] Nahid-Al-Masood, N. Modi, and R. Yan, "Low inertia power systems: Frequency response challenges and a possible solution," in *Australasian Universities Power Engineering Conference (AUPEC)*, Sept 2016.

[4] S. Eftekharnejad, V. Vittal, G. T. Heydt, B. Keel, and J. Loehr, "Impact of increased penetration of photovoltaic generation on power systems," *IEEE Transactions on Power Systems*, vol. 28, no. 2, pp. 893–901, May 2013.

[5] A. M. Azmy and I. Erlich, "Impact of distributed generation on the stability of electrical power system," in *IEEE Power Engineering Society General Meeting, 2005*, June 2005, pp. 1056–1063 Vol. 2.

[6] A. K. Srivastava, A. A. Kumar, and N. N. Schulz, "Impact of distributed generations with energy storage devices on the electric grid," *IEEE Systems Journal*, vol. 6, no. 1, pp. 110–117, March 2012.

[7] M. Ashabani and Y. A. R. I. Mohamed, "Novel comprehensive control framework for incorporating vscs to smart power grids using bidirectional synchronous-vsc," *IEEE Transactions on Power Systems*, vol. 29, no. 2, pp. 943–957, March 2014.

[8] T. V. Van, K. Visscher, J. Diaz, V. Karapanos, A. Woyte, M. Albu, J. Bozelie, T. Loix, and D. Federenciuc, "Virtual synchronous generator: An element of future grids," in *2010 IEEE PES Innovative Smart Grid Technologies Conference Europe (ISGT Europe)*, Oct 2010, pp. 1–7.

[9] S. D'Arco and J. A. Suul, "Virtual synchronous machines - classification of implementations and analysis of equivalence to droop controllers for microgrids," in *2013 IEEE Grenoble Conference*, June 2013, pp. 1–7.

[10] J. Driesen and K. Visscher, "Virtual synchronous generators," in *2008 IEEE Power and Energy Society General Meeting - Conversion and Delivery of Electrical Energy in the 21st Century*, July 2008, pp. 1–3.

[11] M. Ashabani and Y. A. R. I. Mohamed, "Integrating vscs to weak grids by nonlinear power damping controller with self-synchronization capability," *IEEE Transactions on Power Systems*, vol. 29, no. 2, pp. 805–814, March 2014.

[12] H. P. Beck and R. Hesse, "Virtual synchronous machine," in *2007 9th International Conference on Electrical Power Quality and Utilisation*, Oct 2007, pp. 1–6.

[13] S. M. Ashabani and Y. A. R. I. Mohamed, "General interface for power management of micro-grids using nonlinear cooperative droop control," *IEEE Transactions on Power Systems*, vol. 28, no. 3, pp. 2929–2941, Aug 2013.

[14] T. L. Vandoorn, B. Meersman, J. D. M. D. Kooning, and L. Vandevelde, "Directly-coupled synchronous generators with converter behavior in islanded microgrids," *IEEE Transactions on Power Systems*, vol. 27, no. 3, pp. 1395–1406, Aug 2012.

[15] C. Rahmann, J. Jara, and M. B. C. Salles, "Effects of inertia emulation in modern wind parks on isolated power systems," in *2015 IEEE Power Energy Society General Meeting*, July 2015, pp. 1–5.

[16] S. M. Malik, X. Ai, Y. Sun, C. Zhengqi, and Z. Shupeng, "Voltage and frequency control strategies of hybrid ac/dc microgrid: a review," *IET Generation, Transmission Distribution*, vol. 11, no. 2, pp. 303–313, 2017.

[17] J. Svensson, "Synchronisation methods for grid-connected voltage source converters," *IEE Proceedings - Generation, Transmission and Distribution*, vol. 148, no. 3, pp. 229–235, May 2001.

[18] F. B. M. Ciobotaru, R. Teodorescu, "A new single-phase pll structure based on second order generalized integrator," in *2006 37th IEEE Power Electronics Specialists Conference*, June 2006, pp. 1–6.

[19] S. Shinnaka, "A robust single-phase pll system with stable and fast tracking," *IEEE Transactions on Industry Applications*, vol. 44, no. 2, pp. 624–633, March 2008.

[20] L. Harnefors, M. Bongiorno, and S. Lundberg, "Input-admittance calculation and shaping for controlled voltage-source converters," *IEEE Transactions on Industrial Electronics*, vol. 54, no. 6, pp. 3323–3334, Dec 2007.

[21] Q. C. Zhong, P. L. Nguyen, Z. Ma, and W. Sheng, "Self-synchronized synchronverters: Inverters without a dedicated synchronization unit," *IEEE Transactions on Power Electronics*, vol. 29, no. 2, pp. 617–630, Feb 2014.

[22] L. Zhang, L. Harnefors, and H. P. Nee, "Power-synchronization control of grid-connected voltage-source converters," *IEEE Transactions on Power Systems*, vol. 25, no. 2, pp. 809–820, May 2010.

[23] M. Ashabani, F. D. Freijedo, S. Golestan, and J. M. Guerrero, "Inducverters: Pll-less converters with auto-synchronization and emulated inertia capability," *IEEE Transactions on Smart Grid*, vol. 7, no. 3, pp. 1660–1674, May 2016.

[24] Prabha Kundur and P. Kundur, *Power System Stability And Control*. McGraw-Hill Education, 1994.

[25] D. W. N. R. W. De Doncker, "The universal field oriented controller," *IEEE Transactions on Industry Application*, vol. 30, no. 1, pp. 92–100, Jan/Feb 1993.

[26] S. Golestan, F. D. Freijedo, A. Vidal, J. M. Guerrero, and J. Doval-Gandoy, "A quasi-type-1 phase-locked loop structure," *IEEE Transactions on Power Electronics*, vol. 29, no. 12, pp. 6264–6270, Dec 2014.

[27] R. V. Shepherd, "Synchronizing and damping torque coefficients of synchronous machines," *Transactions of the American Institute of Electrical Engineers. Part III: Power Apparatus and Systems*, vol. 80, no. 3, pp. 180–189, April 1961.

[28] S. D'Arco, J. A. Suul, and O. B. Fosso, "Small-signal modelling and parametric sensitivity of a virtual synchronous machine," in *2014 Power Systems Computation Conference*, Aug 2014, pp. 1–9.

[29] J. Liu, Y. Miura, and T. Ise, "Comparison of dynamic characteristics between virtual synchronous generator and droop control in inverter-based distributed generators," *IEEE Transactions on Power Electronics*, vol. 31, no. 5, pp. 3600–3611, May 2016.

[30] Y. Du, J. M. Guerrero, L. Chang, J. Su, and M. Mao, "Modeling, analysis, and design of a frequency-droop-based virtual synchronous generator for microgrid applications," in *2013 IEEE ECCE Asia Downunder*, June 2013, pp. 643–649.

[31] J. Rocabert, A. Luna, F. Blaabjerg, and P. Rodrguez, "Control of power converters in ac microgrids," *IEEE Transactions on Power Electronics*, vol. 27, no. 11, pp. 4734–4749, Nov 2012.

[32] J. C. Vasquez, J. M. Guerrero, A. Luna, P. Rodriguez, and R. Teodorescu, "Adaptive droop control applied to voltage-source inverters operating in grid-connected and islanded modes," *IEEE Transactions on Industrial Electronics*, vol. 56, no. 10, pp. 4088–4096, Oct 2009.

[33] J. G. Ziegler and N. B. Nichols, "Optimum settings for automatic controllers," *Journal of Dynamic Systems, Measurement, and Control*, pp. 220–222, Jun 1993.